ELSEVIER

Catalysis Today 53 (1999) 245–258

CATALYSIS TODAY

www.elsevier.com/locate/cattod

Diffusion and reaction in porous networks

Frerich J. Keil*

Department of Chemical Engineering, Technical University of Hamburg-Harburg, Eissendorfer Strasse 38, D-21073, Hamburg, Germany

Abstract

The present paper reviews three-dimensional random network models of catalyst support structures. Multicomponent diffusion in the individual pores of the network is described by the dusty-gas approach. In contrast to previous publications, the present network model can be applied to any common reaction kinetics. This becomes inevitable in order to make three-dimensional network models applicable to practical problems in the industry. The present model is closely connected to measurable quantities which may be obtained by standard equipment. Examples of pore structure optimizations with respect to various optimization criteria are given. Investigations of depositions within the pores by percolation theoretical methods are described. Results of simulations are compared to measurements in a single-pellet diffusion reactor. The importance of surface diffusion is stressed. ©1999 Elsevier Science B.V. All rights reserved.

Keywords: Network model; Porous media; Multicomponent diffusion; General kinetics; Pore structure optimization

1. Introduction

Although some books on ‘catalyst design’ have already been published (see e.g. [1,2]), there is only a modest progress in catalyst design from the first principles. When modeling phenomena in catalyst particles, one has to solve a variety of difficult problems, like multicomponent diffusion in porous media, surface diffusion, description of porous structures, modeling of the active centers, adsorption, reaction and desorption of reactants and products. At present, only experimental surface science methods (see e.g. Somorjai [3], Woodruff and Delchar [4]) in combination with the methods of experimental kinetics (see e.g. Christoffel [5], Anderson and Dawson [6], Mills and Lerou [7], and Kapteijn and Moulijn [84]) and theoretical chemistry (see e.g. van Santen [8,9], van Santen and Neurock [10]) will give reliable results. Methods of statistical physics like Monte Carlo approaches and molecular dynamics [11] complement the quantum chemical tools. Strategies to model catalytic reactions in terms of elementary chemical reactions that occur on the catalytic surface and their relation with each other and with the surface during a catalytic cycle are given by Dumesic et al. [12] (see also Boudart [13]). Further progress can be expected by employing model systems which incorporate a support but still allow the use of methods from surface science [14].

In the present paper, multicomponent diffusion and reaction within porous catalyst supports will be described. Krishna [15], Krishna and Wesselingh [16], and Taylor and Krishna [17] give an outline of multicomponent diffusion modeling.

Firstly, one has to describe the porous structure of the support and its change with time. Three-dimensional random networks will be used for this purpose. This type of model describes the voidage as interconnected pores with a random distribution of pore sizes. In principle, any shape of pores can be used (e.g. cylindrical, slit-type). The

* *E-mail address:* keil@tu-harburg.de (F.J. Keil)

PII: S0920-5861(99)00119-4

pore size distribution can be obtained experimentally from either nitrogen sorption measurements or mercury porosimetry. These measurements can be evaluated by a variety of methods. Other approaches are statistical mechanical techniques or reconstruction calculations from diffusion experiments in a diffusion cell. The pore walls can be smooth, irregular or even fractal. The distribution of pore radii can also be the result of optimization calculations according to given optimization criteria like, for example, maximum production or maximum operation time.

Secondly, multicomponent diffusion has to be calculated. The common procedure is to employ the dusty-gas model that has been developed by Mason and his co-workers [18]. This model combines molecular diffusion, Knudsen diffusion, viscous flux, and, in principle, surface diffusion. The dusty-gas model is suitable for any model of the porous structure. The fundamentals of surface, configuration and anomalous diffusion are still under investigation. Molecular dynamics and Monte Carlo approaches are the preferred methods of calculation for these transport mechanisms.

Thirdly, the reaction has to be modeled. The general procedure is the fitting of experimental data to a set of rate equations, mostly the of Langmuir–Hinshelwood- or Eley–Rideal-type [19]. As has been demonstrated in a book written by Mezaki and Inoue [20], 98 commercial heterogeneous reactions out of 100 reactions compiled followed a Langmuir–Hinshelwood or a Eley–Rideal rate equation. The reason for this extraordinary success of the two approaches is not clear in detail. As is well known, contrary to the assumptions of the Langmuir–Hinshelwood approach, the adsorption sites are quite different, and various types of lateral interactions occur between the adsorbed species. The lateral interactions between the adsorbates may not be isotropic, the surface may reconstruct, and the reaction itself may cause non-trivial correlations to arise in the distribution of adsorbed species. Contrary to these phenomena, the Langmuir–Hinshelwood rate equation assumes a random distribution of non-interacting reactants. The kinetics of an elementary surface reaction may not bear a simple relationship to the stoichiometry of the reaction, when there are lateral interactions between adsorbed molecules. Examples of these phenomena are reviewed by Kang and Weinberg [21], Masel [22], Boudart and Djéga-Mariadassou [23], among others. Much kinetic data may also be found in Somorjai's book [3]. Why the Langmuir–Hinshelwood kinetics works so well in practice had led to controversies in the literature [24]. The same holds for the concept of turnover frequency (TOF) in heterogeneous catalysis [25]. Boudart [26] gives a review of this approach, and Ribeiro et al. [27] discuss guidelines for experimental work in heterogeneous catalysis that will help to improve the reproducibility of measurements of turnover rates. Weller [28] considers many aspects of heterogeneous kinetics.

One should bear in mind that a good fit of experimental data to a Langmuir–Hinshelwood equation does not mean that this equation reflects the real mechanism of the reaction. This might be the case only by accident.

In the present paper, a network model will be described which allows the application of any common type of reaction kinetics. This becomes quite inevitable in order to make three-dimensional network models applicable to practical problems in industrial catalyst design.

2. Modeling of porous catalyst supports

Surface area and pore structure are two important properties of catalyst supports. Gas reactions catalyzed by solid materials occur on the exterior and mainly interior surfaces of the porous catalyst support. The specific rate of reaction is a function of the accessible surface area. The greater the amount of accessible internal surface area, the larger is the amount of reactant converted per unit time and unit mass of catalyst. A second factor is the porous structure which comprises properties like pore size distribution, connectivity and shape of pores. These factors influence the selectivity of reactions. Owing to possible deposition of molecules, for example carbon deposition, the pore structure may change as a function of time. Finally, the accessibility of the pores will drop to zero, such that the pellet will be catalytically inactive. Proper design of the porous structure may extend the operating time of a catalyst.

Wheeler [29] was one of the first to have considered a pore model. He proposed that the mean radius $\bar{r}$ and the length $\bar{L}$ of pores in a pellet are determined in such

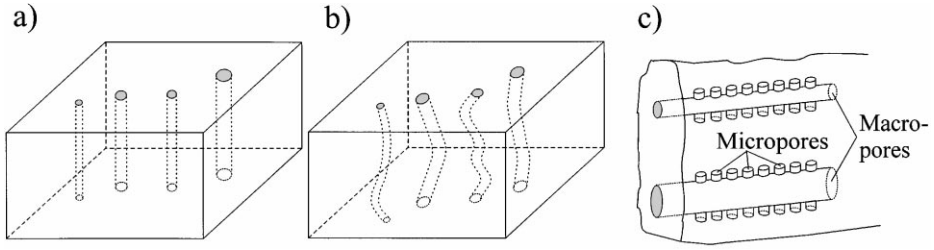

Fig. 1. Parallel pore model (a) straight, (b) tortuous pores, (c) micro/macropore model.

a way that the sum of the surface areas of all the pores constituting the system of pores is equal to the BET surface area, and that the sum of the pore volumes is equal to the experimental pore volume. After some calculations, one obtains for the average pore radius and the average pore length the following equations:

$$\bar{r} = \frac{2V_g}{S_g}\sigma\ (1-\psi) \tag{1}$$

$$\bar{L} = \sqrt{2}\frac{V_p}{S_x} \tag{2}$$

The term V_g presents the specific pore volume, S_g is the BET specific surface area, σ a pore wall roughness factor, ψ the pellet porosity, V_p is the total volume of the catalyst pellet and S_x the external surface area of a catalyst particle. The model provides $\bar{r}$ and $\bar{L}$ in terms of experimentally determinable quantities. The pore surface area determined by adsorption measurements is not a unique value but depends heavily on the models used for the data evaluation. It is generally agreed upon that the nitrogen BET method of measuring the surface area of solids is based on Langmuirian assumptions that are totally unacceptable. Various other methods for the evaluation of pore surface data were developed [30,43]. Current developments in this field are discussed in the Characterization of Porous Solids (COPS) meetings, the results of which are published in the series Studies in Surface Science and Catalysis [31]. One should bear in mind that different methods of data evaluation give different pore surfaces and pore radii distributions, as expected.

In the sixties, some other pore models were created. Slightly more realistic than the Wheeler model are tortuous capillaries (see Fig. 1b). The random-pore model by Wakao and Smith [81] was originally developed for pellets containing a bidisperse pore system, such as alumina. It is supposed that the pellets consist of an assembly of small particles. When the particles themselves contain pores (micropores), there exists both a macro and a micro void-volume distribution. The voids are not imagined as capillaries but more as an assembly of short void regions surrounding and between individual particles. The drawback of this model is the absence of connections between pores. In fact, it is a refined version of a parallel pore model. A similar model was developed by Mann and Thomson [32] (see Fig. 1c). A progress was made by the model of Johnson and Stewart [33] which employs randomly oriented capillary axes and are cross-linked (see Fig. 2). Similar models were also used by Feng and Stewart [34]. In the eighties, Bethe lattices were introduced by Beeckman et al. [35], Beeckman and Froment [36], and Reyes and Jensen [37] (see Fig. 3).

Fig. 2. Pore model by Johnson and Stewart [33].

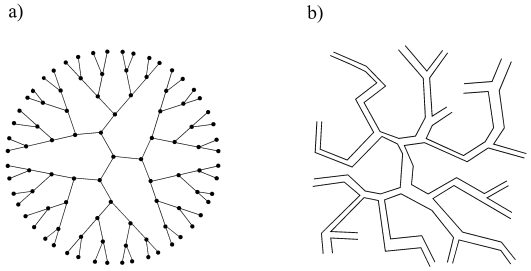

Fig. 3. Bethe lattice (a) coordination number $Z = 3$, (b) a possible corresponding pore structure.

In these models, no closed loops and fixed connectivity are employed. A considerable progress could be achieved by employing random networks. Sharratt and Mann [82] were the first to have extensively studied the properties of these models in connection with diffusion and reaction phenomena. This type of model describes the voidage as interconnected pores with a random distribution of pore sizes (e.g. pore radii for cylindrical pores). The pore size distribution can be obtained experimentally from either nitrogen sorption measurements or mercury porosimetry. Of course, one has to take into consideration the limitations mentioned above. A different approach is the reconstruction of the pore radii distribution by employing diffusion measurements in a Wicke–Kallenbach cell (see Keil and Schreiber [38]). A further very important property is the mean coordination number (connectivity) of the pores. This number may be obtained from the evaluation of the hysteresis of the BET adsorption/desorption curve (Seaton [39], Liu et al. [40]) or the hysteresis of the mercury porosimetry curve [41]. Furthermore, one can use digital image processing for finding the connectivity [42,98]. For this purpose, the support is impregnated by a low-melting point alloy (e.g. Woods metal). After cooling down, the solidified samples are carefully sectioned and polished to reveal a visualization of the penetrated pores. From special techniques, one can obtain the connectivity. As has been found by Hollewand and Gladden [44,45], one should differentiate between distinct but interconnected micro- and macropore networks, to provide a realistic representation of a bimodal porous network. On account of the preparation process, they consist of microporous particles with macropores among them. In Fig. 4a, a two-dimensional cut and a three-dimensional bimodal pellet are presented. In

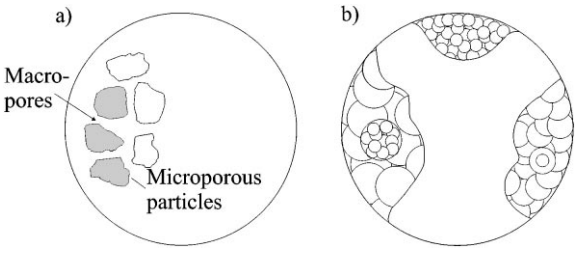

Fig. 4. Catalyst support manufactured by compression of microparticles (a) two-dimensional cut, (b) three-dimensional view.

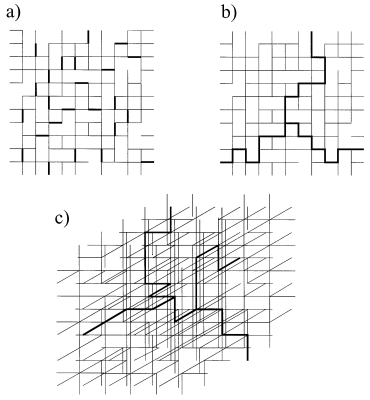

Fig. 5. Cubic random pore models, (a) two-dimensional random micro/macropore network, (b) the macropore network spans the entire network, (c) three-dimensional micro/macropore network, the macropores span the entire network.

Fig. 5a, two- and three-dimensional random cubic networks are given. There is a considerable difference between Fig. 5a and Fig. 5b. In Fig. 5a, the micro- and macropores are randomly distributed, whereas in Fig. 5b, the more realistic case is presented where the macropores cover the entire network. In case of carbon deposition, the network in Fig. 5b will be active for a longer time compared to the network in Fig. 5a. Random three-dimensional pore networks are advantageous in several respects:

1. The effect of connectivity of the pore space is taken into account.
2. Any type of network can be employed (e.g. regular, irregular, Voronoi [46]).
3. Any pore size distribution and any pore geometry, e.g. cylindrical or slit-like pores, can be used.
4. It is possible to model local heterogeneities, e.g. spatial variation in mean pore size. This is an important point, as Hollewand and Gladden [47] detected by pulsed gradient spin echo NMR (PGSE NMR), that the pellets are quite heterogeneous. This fact is also known from measurements in single-pellet diffusion cells.
5. Any distribution of catalytic active centers may be taken into account. Due to various impregnation and reduction methods, the distribution of active centers will be different. This causes different diffusional fluxes inside the pore network.
6. Percolation phenomena can be described. Deactivation processes can be modelled by percola-

tion approaches (see e.g. Sahimi and Tsotsis [48]). An introduction to percolation theory is given by Stauffer and Aharony [49].

7. The pore walls can be smooth, irregular or even fractal. There is some evidence that the pore walls are fractal. Details can be found in the books by Avnir (Ed.) [54] and Rothschild [55].
8. Fitting parameters like tortuosity τ can be avoided. Tortuosity is an ill-defined correction factor which contains all model deficiencies. Its relation to the geometric structure of the pore system is not clear, and the factor is not a constant under reactive conditions. Aris [95] states: "When models are made of the configuration of the pore structure τ can be related to some other geometrical parameter but in general it is a fudge factor of greater or less sophistication".

One has to bear in mind that, in lattice-based models, diffusion and reaction phenomena are limited to the lattice framework. In order to remove this limitation, Drewry and Seaton [50], among others, have modeled porous catalysts as randomly sized and located spheres representing the support and active sites. Pores, pore size distributions, and pore networks are idealizations of the real cavities in the catalyst supports. A two-dimensional cut of a possible real support is presented in Fig. 6. Hesse [51] discussed the influence of the pore length, especially for very short pores, on the transport resistance. Small Knudsen numbers (ratio of the pore diameter to the mean free path of molecules) lead to an increase in the transport resistance. A typical situation is presented in Fig. 7. A narrow pore is connected to a wide pore. The molecules

Fig. 6. Two-dimensional cut of a real catalyst.

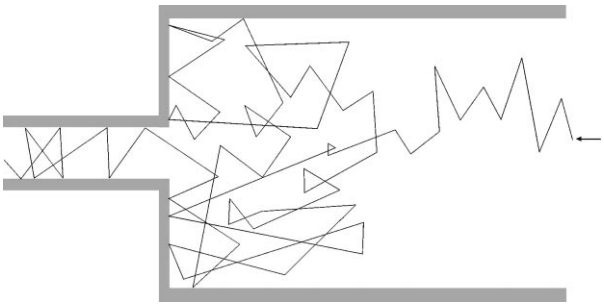

Fig. 7. Trace of a particle in a macropore connected to a micropore.

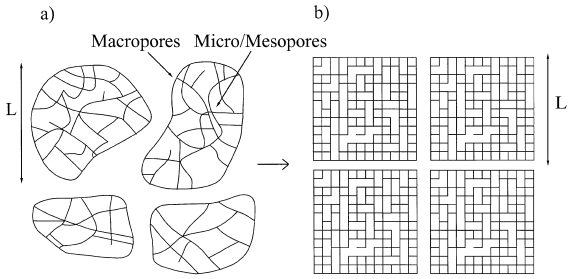

Fig. 8. Mapping of an irregular two-dimensional pore structure onto a regular cubic grid.

are reflected several times until they penetrate the narrow pore which prolongs the diffusion path.

Jerauld et al. [52] and Winterfeld et al. [53] have shown that, as long as the average coordination number of a topologically-disordered system is equal to the coordination number of a regular network, the transport properties of the two systems are essentially identical. A mapping of a disordered structure onto a regular one is shown in Fig. 8. More details about porous structures are given by Dullien [56], Adler [57], Sahimi et al. [58], Keil [59] and Mann [43,60].

In the model presented below, a three-dimensional random cubic network of interconnected cylindrical pores was taken. The pore walls were assumed to be smooth, but the mathematical model can be used for other networks also, like Voronoi grids. Fractal walls can also be employed and different pore geometries can be taken as well. The pore radii are randomly distributed over the network so as to meet a predetermined overall distribution function obtained from nitrogen adsorption measurements. A randomly generated macropore network was introduced which extends throughout the entire pellet augmented by

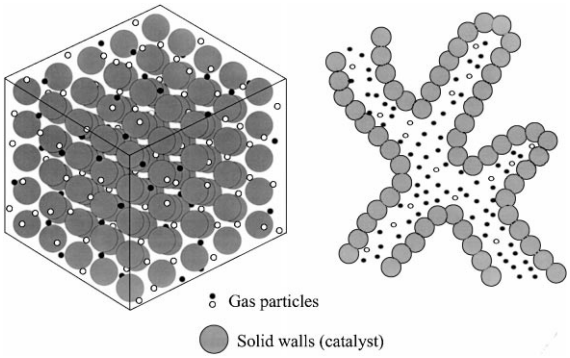

Fig. 9. Dusty-gas model and a two-dimensional cut of some pores.

a micropore network. The network size was from $30 \times 30 \times 30$ to $80 \times 80 \times 80$ nodes.

3. Diffusion and reaction

Multicomponent diffusion in porous media is described by the so-called dusty-gas model [15–17,83] and is based on the Stefan–Maxwell approach for diluted gases which is an approximation of Boltzmann's equation. The pore walls are (see Fig. 9) considered as consisting of giant molecules ('dust') distributed in space. These dust molecules are treated as a pseudo-species $n+1$ in the n-component gaseous mixture. The dust particles are kept fixed in space, and are treated like a gas component in the Stefan–Maxwell equations. Multicomponent diffusion shows some peculiarities which do not occur in binary diffusion. These phenomena were discovered by Toor [61] and were experimentally confirmed by Duncan and Toor [62]. Toor assigned the following names to these curious phenomena:

- Osmotic diffusion: the diffusion of a component takes place despite the absence of a constituent driving force.
- Reverse diffusion: the diffusion of a component takes place in a direction opposite to its driving force; which means that the components flow in the direction opposite to their concentration gradients. This effect was also shown by molecular dynamics [63].
- Diffusion barrier: a component diffusion flux is 0 despite the existence of a large driving force.

These phenomena cannot be described by the Fick formulation of diffusion. Within the pores, we may distinguish three different types of diffusion mechanisms:

- Molecular diffusion: this type becomes significant for large pore sizes and high system pressures; here, molecule–molecule collisions dominate over molecule–wall collisions.
- Knudsen diffusion: this mechanism becomes predominant when the mean free path of the molecular species is much larger than the pore diameter such that molecule–wall collisions become important.
- Surface diffusion: this type describes the movement of physisorbed and chemisorbed molecular or atomic species along the pore wall surface. At elevated pressures, this mechanism contributes considerably to the total flux, as was already observed by Feng and Stewart [64].

In microporous media, the so-called 'configurational diffusion' occurs. Details are, for example, given by Kärger and Ruthven [65], Bell et al. [66], or Keil et al. [67].

Within the pores of a sorbent, one has, in general, a combination of the three diffusion mechanisms mentioned above. The total flux of any species is obtained by combining the separate contributions. The combination can be visualized by an electric analogue circuit as presented in Fig. 10.

In the following section, a model developed by Rieckmann and Keil [68–70] will be given. The basic features of the model are as follows:

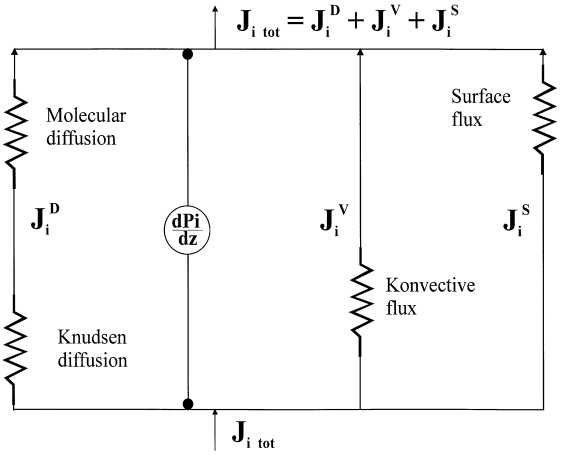

Fig. 10. Electric circuit analogue of diffusive, convective and surface diffusive fluxes.

1. Multicomponent diffusion has been modeled according to the dusty-gas approach.
2. Multicomponent diffusion and reaction occur in a random three-dimensional network of interconnected pores with a predefined average connectivity and distribution of pore radii, whereby any type of network and pores can be employed. An average connectivity of the pores up to 6 can be selected. In practice, most catalyst supports exhibit connectivities between 3 and 6.
3. Percolation phenomena like pore clogging, owing to deposition of carbon or other molecules, can be studied. For this purpose, the network can be investigated by the Hoshen–Kopelman algorithm [71]. With the aid of this algorithm, one can, for example, obtain the accessible surface within the network.
4. Different distributions of active centers can be studied.
5. In contrast to previous work, any common type of reaction kinetics may be applied. This is the most important aspect of the model. In order to make three-dimensional networks applicable to practical problems in the chemical process industry, they have to be suitable for any system of rate equations. Recently developed numerical techniques have led to a considerable reduction of computer memory requirements for such calculations.

The mass transport in the single pores is described according to the dusty-gas model as a sum of diffusive, viscous and surface fluxes (see Fig. 10):

$$\boldsymbol{J} = \boldsymbol{J}^{\mathrm{D}} + \boldsymbol{J}^{\mathrm{V}} + \boldsymbol{J}^{\mathrm{S}} \tag{3}$$

The first term on the right hand side represents the flux due to molecular and Knudsen diffusion:

$$\boldsymbol{J}^{\mathrm{D}} = -(\boldsymbol{D}^{\mathrm{D}}(r_{\mathrm{p}}, \boldsymbol{c}))^{-1} \frac{\mathrm{d}\boldsymbol{c}}{\mathrm{d}w} \tag{4}$$

$$\boldsymbol{D}^{\mathrm{D}}_{ij}(r_{\mathrm{p}}, \boldsymbol{c}) = \begin{cases} -\frac{x_i}{D_{ij}} & \text{for } i \neq j \\ \frac{1}{D^{\mathrm{K}}_{ii}} + \sum_{\substack{h=1 \\ h\neq i}}^{N} \frac{x_h}{D_{ih}(p)} & \text{for } i = j \end{cases} \tag{5}$$

The term x_i represents the mole fraction of component i, D_{ij} the binary molecular diffusivity of components i and j, D^{K}_{ii} the Knudsen diffusivity of component i, $\boldsymbol{c}$ the vector of concentrations, w the length coordinate of the pore, p the pressure, N the number of components, and r_{p} the pore radius. The viscous flux is given by the following expression:

$$\boldsymbol{J}^{\mathrm{V}} = -\boldsymbol{c} \frac{r_{\mathrm{p}}^2}{8\eta} ZRT \frac{c_{\mathrm{tot}}}{\mathrm{d}w} \tag{6}$$

with

$$c_{\mathrm{tot}} = \sum_{i=1}^{N} c_i \tag{7}$$

The expression Z is the compressibility factor, η the dynamic viscosity, R the gas constant, T the temperature, and c_{tot} the total concentration.

The surface diffusion was modeled according to Krishna [72]:

$$\boldsymbol{J}^{\mathrm{S}} = -\boldsymbol{D}^{\mathrm{S}}(\boldsymbol{c}) \frac{\mathrm{d}\theta(\boldsymbol{c})}{\mathrm{d}w} \cdot \frac{2c_l}{r_{\mathrm{p}}} \tag{8}$$

with the surface diffusivity according to

$$\boldsymbol{D}^{\mathrm{S}}(\boldsymbol{c}) = (\boldsymbol{B}^{\mathrm{S}})^{-1} \cdot \boldsymbol{\Gamma} \tag{9}$$

$$\boldsymbol{B}^{\mathrm{S}}_{ij}(\boldsymbol{c}) = \begin{cases} -\frac{\theta_i(\boldsymbol{c})}{D^{\mathrm{S}}_{ij}} & \text{for } i \neq j \\ \frac{1}{D^{\mathrm{S}}_{i}} + \sum_{\substack{h=1 \\ h\neq i}}^{N} \frac{\theta_h(\boldsymbol{c})}{D^{\mathrm{S}}_{ih}} & \text{for } i = j \end{cases} \tag{10}$$

$$\Gamma_{ij}(\boldsymbol{c}) = \delta_{ij} + \frac{\theta_i(\boldsymbol{c})}{1 - \theta_{\mathrm{tot}}(\boldsymbol{c})} \tag{11}$$

$$\theta_{\mathrm{tot}} = \sum_{i=1}^{N} \theta_i \tag{12}$$

The term θ_i represents the fractional surface occupancy of component i, D^{S}_{ij} the countersorption Stefan–Maxwell diffusivity, D^{S}_{i} the surface diffusivity of component i, and c_l the concentration of active centers (adsorption sites).

Chemical reactions occur within the pores. Any system of common rate equations (power law equations, Langmuir–Hinshelwood or Eley–Rideal equations, and others), can be included. Therefore, one finally obtains the following differential material balance for a single pore in axial direction:

$$\frac{\mathrm{d}\boldsymbol{J}}{\mathrm{d}w} - \boldsymbol{\nu} \frac{2}{r_{\mathrm{p}}} \boldsymbol{r}(\boldsymbol{c}, T) = \boldsymbol{0} \tag{13}$$

The expression $\boldsymbol{\nu}$ is the stoichiometric matrix and $\boldsymbol{r}$ the system of rate equations. The other terms have

the same meaning as given above. For isothermal conditions, the temperature, T, is constant. Finally, one obtains for each single pore following the system of second-order differential equations

$$\mathbf{0} = -RT\frac{r_\mathrm{p}^2}{8\eta}\left(\boldsymbol{c}\cdot\frac{\mathrm{d}^2_{tot}}{\mathrm{d}w^2}+\frac{\mathrm{d}\boldsymbol{c}}{\mathrm{d}w}\cdot\frac{\mathrm{d}c_\mathrm{tot}}{\mathrm{d}w}\right)$$
$$-(\boldsymbol{D}^\mathrm{D}(\boldsymbol{c}))^{-1}\cdot\frac{\mathrm{d}^2c}{\mathrm{d}w^2}-\frac{\mathrm{d}}{\mathrm{d}w}((\boldsymbol{D}^\mathrm{D}(\boldsymbol{c}))^{-1})\cdot\frac{\mathrm{d}\boldsymbol{c}}{\mathrm{d}w}$$
$$-\frac{2c_l}{r_\mathrm{p}}\cdot(\boldsymbol{D}^\mathrm{S}(\boldsymbol{c}))^{-1}\cdot\frac{\mathrm{d}^2\theta(\boldsymbol{c})}{\mathrm{d}w^2}-\frac{2c_l}{r_\mathrm{p}}$$
$$\cdot\frac{\mathrm{d}}{\mathrm{d}w}((\boldsymbol{D}^\mathrm{S}(\boldsymbol{c}))^{-1})\cdot\frac{\mathrm{d}\theta(\boldsymbol{c})}{\mathrm{d}w}$$
$$-\boldsymbol{\nu}\cdot\frac{2}{r_\mathrm{p}}\cdot\boldsymbol{r}(c,T) \tag{14}$$

In the three-dimensional pore network, the single pores are connected at the nodes of the network. No adsorption or chemical reaction is assumed to take place at the nodes. The fluxes of each of the species that enter a node must be equal to the fluxes leaving the node. At the inner nodes of the network, an equation similar to Kirchhoff's law holds:

$$\sum_{\substack{k\\ k\varepsilon\, I}}\boldsymbol{J}_k r_{\mathrm{p},k}^2 = 0 \tag{15}$$

where I represents all the pores that are connected at node k, and $\boldsymbol{J}_k$ are the fluxes entering or leaving that node. On the outer surface of the network, a boundary layer is assumed. The flux from the bulk phase into a single pore is

$$\boldsymbol{J} = \beta\,(\boldsymbol{c}_\mathrm{b}-\boldsymbol{c}_\mathrm{S}) \tag{16}$$

The term β is the mass transfer coefficient which may be different for each component. Multicomponent effects may be included. The concentration vectors $\boldsymbol{c}_\mathrm{b}$ and $\boldsymbol{c}_\mathrm{S}$ are for bulk phase and surface, respectively. For each pore of the network, a set of Eq. (14), for each inner node of the network, Eq. (15), and for the outer nodes, Eq. (16) have to be solved. This is done simultaneously for the entire network. The model Eqs. (14)–(16) were solved by a finite difference scheme. The numerical solution is quite difficult. Special techniques like the Schur complement method were employed which reduces the computer storage requirements considerably. In the paper [70], an extension of the Schur complement method is explained which leads to a global convergence of the Newton Algorithm. In the Schur complement approach, the Newton iteration quite often does not converge due to the strong nonlinearity of the systems of equations, caused by the reaction equations. Therefore, a globalization technique, a subspace search with damped vectors, combined with a homotopy method, was developed that guarantees convergence in nearly all cases. In order to cover the entire range of Thiele moduli, the outer dimension of the network has to be similar to the actual pellet size used in operation. Taking a random network of, for example, $100\times100\times100$ nodes with a realistic outer dimension and a pore size distribution like in a real catalyst, leads to a volume ratio of micro- to macropores which is orders of magnitude different from the real one. The same holds for the cross molar fluxes into the pores and porosity of the pellet. Pereira and Beeckman [73] have used an 'exchange term' in their macro-micropore model for the fluxes from the micropores into the macropore. Therefore, one has to scale the fluxes in the following manner:

$$\boldsymbol{J}_\mathrm{M} = \boldsymbol{J}_\mathrm{M,net}\cdot\frac{V_\mathrm{M,cat}}{V_\mathrm{M,net}} \tag{17}$$

$$\boldsymbol{J}_\mathrm{m} = \boldsymbol{J}_\mathrm{m,net}\frac{V_\mathrm{m,cat}}{V_\mathrm{m,net}} \tag{18}$$

$\boldsymbol{J}_\mathrm{M,m}$ are the fluxes within the macro- and micropores, respectively. $V_\mathrm{M,m,cat}$ are the pore volumes of the macro- and micropores of the real catalyst support, whereas $V_\mathrm{M,m,net}$ are the corresponding values for the network. This scaling implies a locally homogeneous pellet structure. If these scalings are omitted, a correct pore structure optimization will not be obtained [74].

The following parameters are employed in the model presented above:

- Pore radii distributions which may be taken from nitrogen adsorption or mercury porosimetry measurements. As already mentioned above, the pore radii distribution one obtains depends on the method of data evaluation, which themselves imply different pore structure models (see e.g. Zgrablich et al. [75], Conner et al. [76]).
- Connectivity found by the method of Seaton [39].
- Kinetic rate expressions from measurements in a Berty reactor or any other suitable type of reactor [84]. The intrinsic rate equations have to be found.

- Transport parameters like binary diffusivities obtained from correlations, e.g. according to Chapman and Enskog, augmented by mixing rules (see e.g. Reid et al. [77]).
- Fugacities and compressibility factors were calculated with the aid of equations of state, for example, the Soave equation.

The model presented is closely connected to measurable quantities, which may be obtained by standard devices. Also, different network models may be found in the literature (see e.g. Sotirchos and Burganos [78], Deepak and Bhatia [79], Reyes and Iglesia [80]).

4. Applications

The model presented above and some simplifications for first-order reactions were applied to different problems in chemical reaction engineering. First, the optimization of a hydrodemetallation (HDM) catalyst will be presented (Keil and Rieckmann [74,85]). Catalytic HDM of crude oil was used for optimization of the pore structure of catalyst supports. Crude oil contains small quantities of nickel and vanadium in the form of porphyrins, in which the metal atom is surrounded by four pyrrole-type rings, and a wide variety of organometallic complexes. Representative concentrations in the atmospheric residue are 6–114 ppm nickel and 30–400 ppm vanadium. During the demetallation process, the metals are deposited on the catalyst in the form of sulfides. These sulfides cause irreversible fouling. The deposits are also active demetallation catalysts but have an activity of only about 80% of the fresh catalyst. As the deposits catalyze demetallation, the pores become more and more filled with deposits, and finally, they will be blocked. Agrawal and Wei [86,87] have investigated kinetics of the HDM reaction of nickel(II) and vanadyl(IV) etioporphyrin I over the $CaO–MoO_3/Al_2O_3$ catalyst in a high-pressure liquid-phase flow reactor. They have found that three major steps are involved. The first step is hydrogenation to intermediates with a first-order dependence on the metal etioporphyrin concentration in the solution and a first-order dependence on hydrogen pressure. The second reaction is the reversible dehydrogenation of the concentration of intermediates in solution with zero-order dependence on hydrogen pressure. The third reaction is the irreversible hydrogenolysis of the intermediates and demetallation, which shows first-order dependence on the intermediate concentration and second-order dependence on the hydrogen pressure. The reaction scheme is as follows:

$$\mathrm{A} \underset{k_2}{\overset{k_1}{\Leftrightarrow}} \mathrm{B} \xrightarrow{k_3} \mathrm{C} \tag{19}$$

Pereira and Beeckman [96] and Pereira [97] have employed a simplified pseudo-first-order kinetics:

$$g = kC_\mathrm{A} \tag{20}$$

where k is the first-order rate constant and C_A is the feed metal concentration. For systems of first-order calculations, analytic solutions for the fluxes may be obtained by, e.g. Laplace transformation, although the calculations become quite tedious for complicated reaction schemes. The solutions for kinetics (19) and (20) are given in Rieckmann et al. [88]. During the process of demetallation, the pores get more and more plugged and the diameters of diffusing molecules come close to the diameters of pore radii. This leads to a so-called hindered diffusion which has been discussed by Deen [89]. The diffusivities were calculated according to Spry and Sawyer [90]:

$$D_\mathrm{A} = D_\infty \left(1 - \frac{r_\mathrm{mol}}{r_\mathrm{p}}\right)^4 \tag{21}$$

where D_∞ is the bulk diffusivity, r_mol the radius of the diffusing molecule and r_p the pore radius at a certain time t. The details of the models are given in the papers [74,85,88]. The models were employed for the optimization of the pore structure of the support according to a performance index, which was the mole flow of the product over a certain period of time:

$$\frac{1}{t}\sum_{i=0}^{n} N_\mathrm{Atot}\,\Delta t_i = \mathrm{MAX!} \tag{22}$$

where N_Atot is the total flux of metal-bearing molecules into the pellet, Δt_i are the time increments, and t the total operating time. Independent variables were the radii of micropores r_m and the microporosity ε_m. These values were bound as follows:

$$25\,\text{Å} \le r_\mathrm{m} \le 150\,\text{Å} \qquad 0.05 \le \varepsilon_\mathrm{m} \le 0.65 \tag{23}$$

As the radii of macropores have far less effect upon the result, only the micropores have been taken as independent variables. The total porosity of the pellet

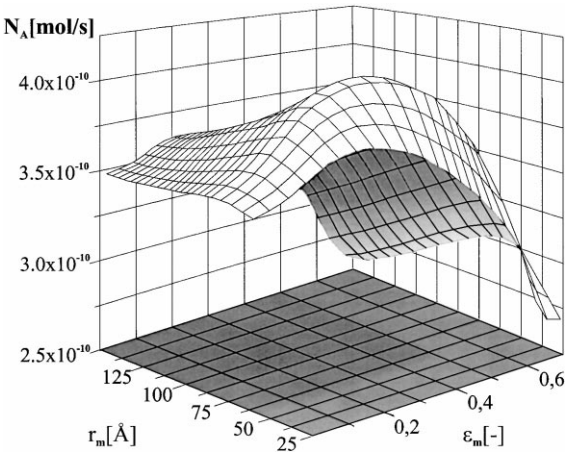

Fig. 11. Optimization of an HDM catalyst [74].

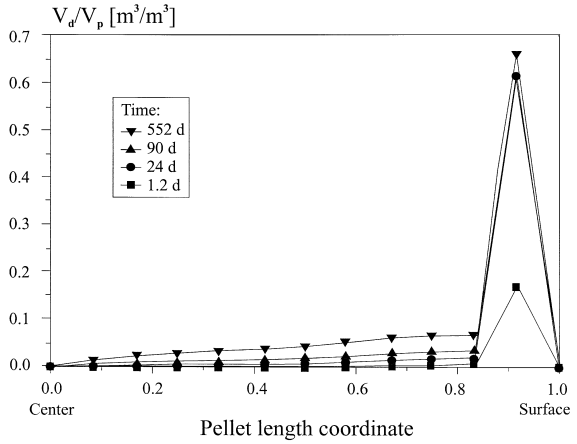

Fig. 12. Deposition profiles at different times in an HDM pellet [88].

was kept fixed at 0.7. In Eq. (22), the mole flow into the pellet is maximized. This is equivalent to a maximum demetallation over a given period of time. The optimization was done with the aid of the COMPLEX method by Box [90]. Other routines, like, e.g. the sequential quadratic programming could also have been used. In Fig. 11 [74], an example for the optimum ($r_{m,opt}$) structure of a demetallation catalyst, which can be produced by using suitable templates, a controlled sol–gel process and certain tempering techniques, is given. Pore structure optimizations improve the performance of catalysts considerably. Hegedus [91] employed the random pore model of Wakao and Smith [81] to optimize the pore structure of automobile exhaust catalysts. A further example of computer-aided design of catalyst support pore structures has been given by Pereira et al. [92]. A model of monolith-type catalysts has been used together with an optimization procedure to maximize the steady-state diffusion controlled catalytic performance after 1000 h of operation in the presence of poisons. Beeckman and Hegedus [93] have developed a model to describe the reduction of NO with NH_3 in simulated power plant stack gases, over the internal surfaces of monolith-shaped catalysts of the vanadia–titania type. The model indicated that up to 50% improvement in the volumetric activity of these catalysts would be possible if they could be prepared with the computed optimum pore structure. Beeckman and Hegedus have found that certain grades of silica could be engineered to satisfy the calculated pore structure requirements.

In the HDM process, after each time step, the pore radii of the network decrease because of the deposits. Parts of the network may be no more accessible from the outer surface. To identify these isolated pore clusters and to calculate the accessible pore space, the network was analyzed by means of percolation theory [88]. The clusters of certain sizes are counted and summarized, pellet spanning clusters are detected and the clusters in contact with the bulk phase are identified by the Hoshen–Kopelman algorithm [49,71]. In Fig. 12, the deposition profiles inside the pellet at different times are presented. The kinetics of Eq. (19) were used. These metal deposition profiles can be studied experimentally by X-ray spectroscopy [87]. The simulations agree with measurements. In Fig. 13, the accessible pore volume is presented as a function of time. After an initial decrease, the mole fluxes and the accessible pore volume remain nearly constant for a long period of time. They drop to zero as the macropores get clogged. This happens after about a year and a half, in accordance with industrial experience. Therefore, the present model allows, based on the experimental data mentioned above, the prediction of the catalyst operating time. This feature of the model makes it useful in catalyst support design. A further example of a coking was investigated in connection with the dehydrogenation of 1-butene to butadiene [68] and a coking reaction [69] described by Beyne and Froment [94].

To test the performance of the network model described above, the computations with this model were compared to experimental results obtained in a

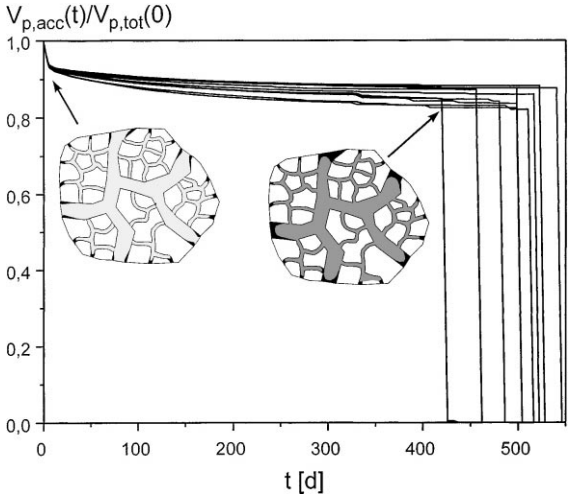

Fig. 13. Normalized accessible pore volume vs. time, 10 different network realizations are presented, depositions at the pore mouths can be observed.

single-pellet diffusion reactor [70]. As an example, the selective hydrogenation of 1,2-dichloropropane to propane and hydrochloric acid was employed:

$$H_6C_3Cl_2 + 2H_2 \rightarrow C_3H_8 + 2\,HCl \tag{24}$$

The intrinsic kinetics was determined with the aid of a Berty reactor. The kinetics could be fitted to a Langmuir–Hinshelwood rate expression. By employing the experimental data as described in Section 2, a very good agreement between experiment and simulation could be obtained. No further readjustments of parameters were made. In Fig. 14, calculated concentration profiles and measurements are presented. No surface diffusion was taken into account in Fig. 14. The measurements coincide with the calculations, except for hydrochloride. Hydrochloride could not be measured properly as it adsorbed strongly on the column in the chromatograph. In Fig. 15, the results of the computations of the pellet center concentrations are shown as a function of pressure. In Fig. 15, the surface diffusivities were included. The model developed by Krishna [72] was employed (see Eqs. (8)–(12)). The surface coverages were modeled according to the Langmuir isotherm:

$$\theta = \frac{Kp}{1 + Kp} \tag{25}$$

The adsorption constants, K, were measured by a chromatographic method and fitted to an Arrhenius formula:

$$K(T) = K^0 \exp\left(\frac{E_{ads}}{RT}\right) \tag{26}$$

The surface diffusivities range from 10^{-9} to 10^{-7} m^2/s (see Satterfield [99]). For propane, the surface diffusivities, D^S, were varied from 8.17×10^{-9}

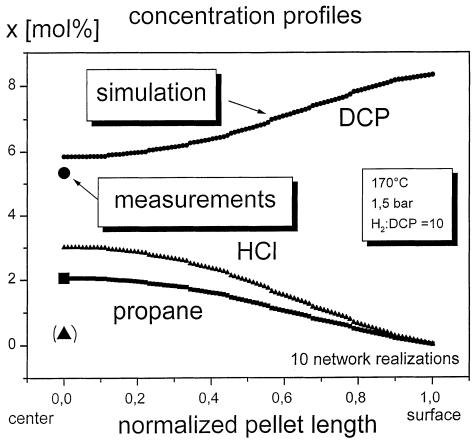

Fig. 14. Calculated concentration profiles and measured center concentrations [70].

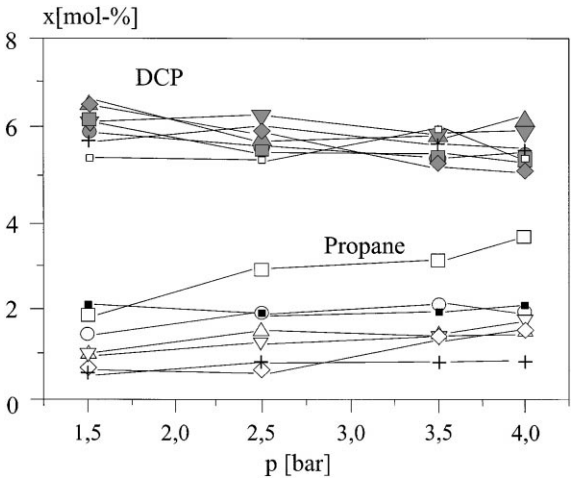

Fig. 15. Calculated center concentrations for various surface diffusion coefficients compared to measurements [70] at 180°C, H_2 : DCP = $10 \times D^S/D^D = 0$ (■), 1×10^{-3} (●), 1.5×10^{-3} (▲), 2.0×10^{-3} (▼), 3.0×10^{-3} (◆), 6.0×10^{-3} (+), and experimental data (□).

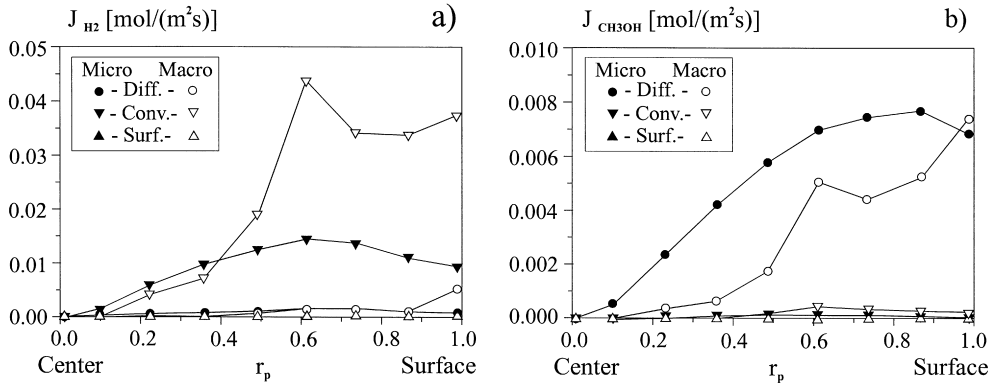

Fig. 16. Diffusive, convective and surface diffusive contributions to the total flux into a catalyst pellet in which methanol synthesis occurs, (a) hydrogen, (b) methanol.

to $8.17 \times 10^{-7}\,m^2/s$, which corresponds to 1/1000 to 1/10 of the molecular diffusivity of propane, respectively. The surface diffusivity of dichloropropane was set equal to 1/1000 of its molecular diffusivity ($1.934 \times 10^{-9}\,m^2/s$), and for hydrochloride, equal to 1/1000 ($3.18 \times 10^{-9}\,m^2/s$). The cross-surface diffusivities were calculated according to

$$D_{ij}^{S} = \sqrt{D_{ii}^{S} D_{jj}^{S}} \tag{27}$$

The total number of active centers in a catalyst support is about 10^{15} centers/cm^2 (see Boudart and Djéga-Mariadassou [23]). Therefore, in the present calculations, a concentration of the active centers, c_l, of $1.6 \times 10^{-5}\,mol/m^2$ was employed. A very good agreement between measurement and calculation could be obtained for a ratio of D^S/D^D of 1.5×10^{-3}, which corresponds to a surface diffusivity for propane of $1.22 \times 10^{-8}\,m^2/s$, a very reasonable value. If the surface diffusion is omitted, the mole fraction of propane is too high for higher pressures. This deviation is due to the stronger adsorption of propane at elevated pressure. The more polar dichloropropane adsorbs strongly even at low pressures. This example clearly demonstrates that the surface diffusion has to be included into the model. This was already observed by Feng and Stewart [34], and has been confirmed in many other examples.

Fig. 16 presents a further important phenomenon. The diffusive, convective and surface diffusive contributions to the total flux in a pellet are given in which a methanol reaction occurs. As the number of moles changes during the reaction, the convective contribution, especially for hydrogen, is quite high. The flux of hydrogen passes mainly through the macropores. For methanol, the diffusive transport dominates. An important point should be stressed. The transport in micro- and macropores is, for methanol, nearly the same. It is quite often assumed that, under stationary conditions, the transport in the macropores dominates. They are called ‘transport pores’. This is correct under nonreactive conditions, but not in case of chemical reactions. Here, the micropores contribute equally to the flux.

5. Conclusions

It has been demonstrated that three-dimensional random networks can contribute considerably to the design of optimum porous structures. These models have to include a proper description of multicomponent diffusion and general systems of rate equations. Investigations by percolation theoretical approaches give insight into deactivation phenomena owing to the deposition of material. These models, combined with some experimental data, have predictive power.

Acknowledgements

The author is grateful to the BMBF for financial support (Grant No. 03D0015A) and the Fonds der Chemischen Industrie.

References

[1] E. R. Becker, C.J. Pereira (Eds.), Computer-Aided Design of Catalysts, Marcel Dekker, New York, 1993.
[2] L.L. Hegedus (Ed.), Catalyst Design, Wiley, New York, 1987.
[3] G.A. Somorjai, in: Introduction to Surface Chemistry and Catalysis, Wiley, New York, 1994.
[4] D.P. Woodruff, T.A. Delchar, Modern Techniques of Surface Science, 2nd ed., Cambridge University Press, Cambridge, UK, 1994.
[5] E.G. Christoffel, Laboratory Studies of Heterogeneous Catalytic Processes, Elsevier, Amsterdam, 1989.
[6] R.B. Anderson, P.T. Dawson (Eds.), Experimental Methods in Catalytic Research, Academic Press, New York, 1976 (three volumes).
[7] P.L. Mills, J.J. Lerou, Rev. Chem. Eng. 9 (1993) 1.
[8] R.A. van Santen, Theoretical Heterogeneous Catalysis, World Scientific, Singapore, 1991.
[9] R.A. van Santen, Chem. Eng. Sci. 45 (1990) 2001.
[10] R.A. van Santen, M. Neurock, Catal. Rev.-Sci. Eng. 37 (1995) 557.
[11] D. Frenkel, B. Smit, Unterstanding Molecular Simulation, Academic Press, San Diego, 1996.
[12] J.A. Dumesic, D.F. Rudd, L.M. Aparicio, J.E. Rekoske, A.A. Treviño, The Microkinetics of Heterogeneous Catalysis, American Chemical Society, Washington, DC, 1993.
[13] M. Boudart, in: G. Ertl, H. Knözinger, J. Weitkamp (Eds.), Handbook of Heterogeneous Catalysis, VCH, New York, p. 958.
[14] P.L.J. Gunter, J.W.H. Niemantsverdriet, F.H. Ribeiro, G.A. Somorjai, Catal. Rev.-Sci. Eng. 39 (1997) 77.
[15] R. Krishna, Chem. Eng. Sci. 48 (1993) 845.
[16] R. Krishna, J.A. Wesselingh, Chem. Eng. Sci. 52 (1997) 861.
[17] R. Taylor, R. Krishna, Multicomponent Mass Transfer, Wiley, New York, 1993.
[18] E.A. Mason, A.P. Malinauskas, Gas Transport in Porous Media, Elsevier, Amsterdam, 1983.
[19] G.F. Froment, L. Hosten, in: J.R. Anderson, M. Boudart (Eds.), Catalysis: Science and Technology, vol. 2, Springer, Heidelberg, 1980, p. 97.
[20] R. Mezaki, H. Inoue, Rate Equations of Solid-Catalyzed Reactions, University of Tokyo Press, Tokyo, 1991.
[21] H.C. Kang, W.H. Weinberg, Chem. Rev. 95 (1995) 667.
[22] R.I. Masel, Principles of Adsorption and Reaction on Solid Surfaces, Wiley, New York, 1996, Chapter 7.
[23] M. Boudart, G. Djéga-Mariadassou, Kinetics of Heterogeneous Catalytic Reactions, Princeton University Press, Princeton, NJ, 1984.
[24] M. Boudart, Ind. Eng. Chem. Fundam. 25 (1986) 656.
[25] G.C. Bond, J. Catal. 136 (1992) 631.
[26] M. Boudart, Chem. Rev. 95 (1995) 661.
[27] F.H. Ribeiro, A.E.S. von Wittenau, C.H. Bartholomew, G.A. Somorjai, Catal. Rev.-Sci. Eng. 39 (1997) 49.
[28] S.W. Weller, Catal. Rev.-Sci. Eng. 34 (1982) 227.
[29] A. Wheeler, Adv. Catal. 3 (1951) 249.
[30] S.J. Gregg, K.S.W. Sing, Adsorption, Surface Area and Porosity, Academic Press, London, 1982.
[31] K.K. Unger, J. Rouquerol, K.S.W. Sing, H. Kral (Eds.), Characterisation of Porous Solids, Stud. Surf. Sci. Catal., vol. 39, Elsevier, Amsterdam, 1988 (see also subsequent volumes).
[32] R. Mann, G. Thomson, Chem. Eng. Sci. 42 (1987) 555.
[33] M.F.L. Johnson, W.E. Stewart, J. Catal. 4 (1965) 248.
[34] C. Feng, W.E. Stewart, Ind. Eng. Chem. Fundam. 12 (1973) 143.
[35] J.W. Beeckman, G.F. Froment, L. Pismen, Chem.-Ing.-Tech. 50 (1978) 960 (in German).
[36] J.W. Beeckman, G.F. Froment, Chem. Eng. Sci. 35 (1980) 805.
[37] S. Reyes, K. Jensen, Chem. Eng. Sci. 40 (1985) 1723.
[38] F.J. Keil, D. Schreiber, Chem.-Ing.-Tech. 66 (1994) 201 (in German).
[39] N.A. Seaton, Chem. Eng. Sci. 46 (1991) 1895.
[40] H. Liu, L. Zhang, N.A. Seaton, Chem. Eng. Sci. 47 (1992) 4393.
[41] R.L. Portsmouth, L. Gladden, Chem. Eng. Sci. 46 (1991) 3023.
[42] R. Scharfenberg, K. Meyerhoff, D. Hesse, Chem. Eng. Sci. 51 (1996) 1889.
[43] R. Mann, A. Al-Lamy, A. Holt, Trans. I. Chem. E 73 (1995) 147.
[44] M.P. Hollewand, L. Gladden, Chem. Eng. Sci. 47 (1992) 1761.
[45] M.P. Hollewand, L. Gladden, Chem. Eng. Sci. 47 (1992) 2757.
[46] A. Okabe, B. Boots, K. Sugihara, Spatial Tessalinations: Concepts and Applications of Voronoi Diagrams, Wiley, New York, 1992.
[47] M.P. Hollewand, L. Gladden, Chem. Eng. Sci. 50 (1995) 309.
[48] M. Sahimi, T. Tsotsis, J. Catal. 96 (1985) 552.
[49] D. Stauffer, A. Aharony, Introduction to Percolation Theory, Taylor & Francis, London, 1992.
[50] H.P.G. Drewry, N.A. Seaton, AIChE J. 41 (1995) 880.
[51] D. Hesse, Chem.-Ing.-Tech. 45 (1973) 442.
[52] G.R. Jerauld, J.C. Hatfield, L.E. Scriven, H.T. Davis, J. Phys. C 17 (1984) 1519.
[53] P.H. Winterfeld, L.E. Scriven, H.T. Davis, J. Phys. C 14 (1982) 2361.
[54] D. Avnir (Ed.), The Fractal Approach to Heterogeneous Chemistry, Wiley, Chichester, UK, 1989.
[55] W. Rothschild, Fractals in Chemistry, Wiley, New York, 1998.
[56] F.A.L. Dullien, Porous Media – Fluid Transport and Pore Structure, North-Holland, Amsterdam, 1992.
[57] P.M. Adler, Porous Media – Geometry and Transports, Butterworth–Heinemann, Boston, 1992.
[58] M. Sahimi, G.R. Gavalas, T.T. Tsotsis, Chem. Eng. Sci. 45 (1990) 1443.
[59] F.J. Keil, Chem. Eng. Sci. 51 (1996) 1543.
[60] R. Mann, in: A. Cybulski, J.A. Moulijn (Eds.), Structured Catalysts and Reactors, Marcel Dekker, New York, 1998.
[61] H.L. Toor, AIChE J. 3 (1957) 198.
[62] J.B. Duncan, H.L. Toor, AIChE J. 8 (1962) 38.
[63] A.P. Thomson, D.M. Ford, G.S. Heffelfinger, J. Chem. Phys. 109 (1998) 6406.
[64] C. Feng, W.E. Stewart, Ind. Eng. Chem. Fundam. 12 (1973) 143.

[65] J. Kärger, D.M. Ruthven, Diffusion in Zeolites and other Microporous Solids, Wiley, New York, 1992.
[66] A.T. Bell, E.J. Maginn, D.N. Theodorou, in: G. Ertl, H. Knözinger, J. Weitkamp (Eds.), Handbook of Heterogeneous Catalysis, vol. 3, VCH, New York, 1997, p. 1165.
[67] F.J. Keil, J. Hinderer, A.R. Garayhi, Catal. Today 50 (1999) 637.
[68] C. Rieckmann, F.J. Keil, Hung. J. Ind. Chem. 24 (1996) 295.
[69] C. Rieckmann, F.J. Keil, Ind. Eng. Chem. Res. 36 (1997) 3275.
[70] C. Rieckmann, F.J. Keil, Chem. Eng. Sci., in press.
[71] J. Hoshen, R. Kopelman, Phys. Rev. B 24 (1976) 3438.
[72] R. Krishna, Chem. Eng. Sci. 45 (1990) 1779.
[73] C.J. Pereira, J.W. Beeckman, Ind. Eng. Chem. Res. 28 (1989) 422.
[74] F.J. Keil, C. Rieckmann, Chem. Eng. Sci. 49 (1994) 4811.
[75] G. Zgrablich, S. Mendioroz, L. Daza, J. Pajares, V. Mayagoitia, F. Rojas, W.C. Conner, Langmuir 7 (1991) 779.
[76] W.C. Conner, S. Christensen, H. Topsoe, M. Ferrero, A. Pullen, in: J. Rouquerol, F. Rodriguez-Remoso, K.S.W. Sing, K.K. Unger (Eds.), Characterization of Porous Solids III, Elsevier, Amsterdam, 1994, p. 151.
[77] R.C. Reid, J.M. Prausnitz, B.E. Poling, The Properties of Gases and Liquids, McGraw-Hill, New York, 1987.
[78] S.V. Sotirchos, V.N. Burganos, AIChE J. 34 (1988) 1106.
[79] P.D. Deepak, S.K. Bhatia, Chem. Eng. Sci. 49 (1994) 245.
[80] S.C. Reyes, E. Iglesia, J. Catal. 9 (1991) 457.
[81] N. Wakao, J.M. Smith, Chem. Eng. Sci. 17 (1962) 825.
[82] P.N. Sharratt, R. Mann, Chem. Eng. Sci. 42 (1987) 1565.
[83] A. Burghardt, Chem. Eng. Process. 21 (1986) 229.
[84] F. Kapteijn, J.A. Moulijn, in: G. Ertl, H. Knözinger, J. Weitkamp (Eds.), Handbook of Heterogeneous Catalysis, vol. 3, VCH, New York, 1997, p. 1189.
[85] F.J. Keil, C. Rieckmann, Hung. J. Ind. Chem. 21 (1993) 277.
[86] R. Agrawal, J. Wei, Ind. Eng. Chem. Process Des. Dev. 23 (1984) 505.
[87] R. Agrawal, J. Wei, Ind. Eng. Chem. Process Des. Dev. 23 (1984) 515.
[88] C. Rieckmann, T. Düren, F.J. Keil, Hung. J. Ind. Chem. 25 (1997) 137.
[89] W.M. Deen, AIChE J. 33 (1987) 1409.
[90] M.J. Box, Computer J. 8 (1965) 42.
[91] L.L. Hegedus, Ind. Eng. Chem. Prod. Des. Dev. 19 (1980) 533.
[92] C.J. Pereira, J.E. Kubsh, L.L. Hegedus, Chem. Eng. Sci. 43 (1988) 287.
[93] J.W. Beeckman, L.L. Hegedus, Ind. Eng. Chem. Res. 30 (1991) 969.
[94] A.O. Beyne, G.F. Froment, Chem. Eng. Sci. 48 (1993) 503.
[95] R. Aris, The Mathematical Theory of Diffusion and Reaction in Permeable Catalysts, vol. 1, Clarendon Press, Oxford, 1975, p. 25.
[96] C.J. Pereira, J.W. Beeckman, Ind. Eng. Chem. Res. 29 (1990) 520.
[97] C.J. Pereira, Ind. Eng. Chem. Res. 29 (1990) 512.
[98] M. Yanuka, F.A.L. Dullien, D.E. Elrick, J. Colloid Interface Sci. 112 (1986) 24.
[99] C.N. Satterfield, Mass Transfer in Heterogeneous Catalysis, Robert E. Krieger Publ., New York, 1981.